



Photon avalanche in lanthanide doped nanoparticles for biomedical applications: super-resolution imaging

Journal:	<i>Nanoscale Horizons</i>
Manuscript ID	NH-COM-02-2019-000089.R1
Article Type:	Communication
Date Submitted by the Author:	19-Mar-2019
Complete List of Authors:	<p>Bednarkiewicz, Artur; Institute of Low Temperature and Structure Research, Polish Academy of Sciences, Excited State Spectroscopy Department; Wroclaw Research Centre EIT+, Department of Nanotechnology</p> <p>Chan, Emory; Lawrence Berkeley National Laboratory, The Molecular Foundry</p> <p>Kotulska, Agata; Institute of Low Temperature and Structure Research, Polish Academy of Sciences, Excited State Spectroscopy Department</p> <p>Marciniak, Lukasz; Polish Academy of Sciences, Institute of Low Temperature and Structure Research</p> <p>Prorok, Katarzyna; WROCLAW RESEARCH CENTRE EIT+,</p>

Photon avalanche phenomenon in lanthanides has been studied in bulk materials towards up-converting lasers, but little is known about the properties and possible applications of this unusual phenomenon at nanoscale. Scarce literature reports suggest the capability of photon avalanche to improve the brightness and deep tissue imaging of extremely photo-stable luminescent nano-labels for biomedical imaging, by diminishing concentration quenching between lanthanide dopants.

Based on theoretical modelling, a new concept of sub-diffraction imaging has been proposed, which exploits highly nonlinear luminescent properties of photon avalanche in nanomaterials under non-resonant photoexcitation. The predicted properties support the assertion that single photoexcitation beam (no depletion beam, as opposed to standard STED) raster imaging at near infrared photoexcitation shall enable to reach below 50 nm optical resolution. This features shall be achievable in a simple optical scheme of widespread conventional or Nipkow disk confocal microscopes, which potentially offers wider adoption of super-resolution imaging in biomedical sciences. The consequences of our studies are much broader and other potential target applications include bio-sensing, optical computing as well as optical thermometry. The current challenge is to experimentally verify the concept by searching for appropriate luminescent materials showing photon avalanche in room temperature at nanoscale.

Photon avalanche in lanthanide doped nanoparticles for biomedical applications: super-resolution imaging

Artur Bednarkiewicz^{1,2*}, Emory Chan³, Agata Kotulska^{1,2},
Lukasz Marciniak², Katarzyna Prorok^{1,2}

1. PORT Polish Center for Technology Development, Wroclaw, Poland
2. Institute of Low Temperature and Structure Research, Polish Academy of Sciences, Wroclaw, Poland
3. The Molecular Foundry, Lawrence Berkeley National Laboratory, Berkeley, CA 94720, USA

*Corresponding author: a.bednarkiewicz@intibs.pl

Confocal fluorescence microscopy is a powerful tool for visualizing biological processes, but conventional laser scanning confocal microscopy cannot resolve structures below the diffraction limit of light. Although numerous sub-diffraction imaging techniques have been developed over last decade, they are still limited by the photobleaching of fluorescent probes and by their complex instrumentation and alignment procedures. To address these issues, we propose a novel concept that relies on using photon avalanche (PA) anti-Stokes emission nanoparticles as luminescent labels. This technique leverages the highly non-linear relationship between photoluminescence intensity and excitation intensity observed with PA, which narrows the point spread function below 50 nm when the non-linearity exceeds 50. Using theoretical modeling, we evaluate the feasibility of obtaining PA in Nd³⁺ doped nanoparticles under non-resonant 1064 nm photoexcitation and study the impact of phenomenological parameters, such as photoexcitation intensity, concentration of dopants or features of the host matrix, on the theoretical PA behavior. Using these optimized parameters, our simulations resolved 20-nm features using non-linear orders of 80. These predictions require experimental proof of concept, which must be preceded by development of

appropriate PA nanomaterials and experimental conditions to observe PA in nanoparticles in room temperature. When successful, the PA phenomenon in bio-functionalized nanoparticles shall radically simplify the technical means for super-resolution imaging.

1. Introduction

Optical microscopy is the most enlightening and intuitive technique for visualizing dynamic processes in biology or revealing cellular function, but the resolution of conventional optical microscopes is limited by the diffraction of light. For visible light, the diffraction limit is approximately one-half of the photoexcitation wavelength along lateral (X-Y) plane and three times larger along the optical axis (Z).^[1] For many biological applications such resolution is insufficient to resolve molecular constructs such as antibodies labelled with fluorescent proteins (e.g. IgG-AlexaFluor 488 has a hydrodynamic size of 12 nm)^[2] or such subcellular structures as ribosomes, dendritic spines or cytoskeleton in neurons.^[3] The resolution suffers in particular when NIR excitation, with its reduced scattering and lower propensity to excite autofluorescence, is used to penetrate through thick layers of tissue. Two-Photon Microscopy (**Figure 1a**) offers increased penetration depths, better point spread function (PSF) confinement and spatial resolution improvement under NIR photoexcitation, but powerful, costly and cumbersome femtosecond lasers must be used due to the low 2- or 3- photon absorption cross-sections of fluorophores (both endogenous or exogenously administrated).^[4,5] Recent advances in far-field super-resolution techniques (e.g., Stimulated Emission Depletion (STED) microscopy, Photo Activated Localisation Microscopy (PALM), Stochastic Optical Reconstruction Microscopy (STORM), 4Pi microscopy, and Structured Illumination)^[6,7] have demonstrated that diffraction limits can be overcome through a combination of smart optical design, novel photon excitation and detection schemes, the selection of specialized fluorescent labels and dedicated data processing.^[6] For example, the concept underlying STED is straightforward and outputs raw data analogous to confocal

micrographs. However, this technique is technically challenging, requiring the synchronization of femtosecond pulses, specialized probes with high stimulated emission (SE) cross section, high depletion excitation intensities leading to fast photobleaching and bio-incompatibility. Despite great progress these areas in the last ten years^[1] (e.g. CW STED^[8], time-gated^[9] or multi-colour STED^[10,11]), alternative techniques and labels are continuously sought.

Luminescent inorganic nanoparticles^[12] have been proposed to counter the photobleaching of conventional fluorescent labels.^[13] Of particular interest, lanthanide doped nanoparticles have been recently proposed for STED,^[14–16] Saturation^[17] or Fluorescence Difference Microscopy (FED)^[18] super-resolution imaging. Tm³⁺ and Yb³⁺ co-doped NaYF₄ “upconverting” nanoparticles (UCNPs) were used as STED probes to image the subcellular cytoskeleton of HeLa cancer cells with 28 nm imaging resolution with 980 nm photoexcitation and 810 nm depletion beams.^[15] The combination of STED with UCNPs is advantageous because they can be imaged in the absence of background (no absorption or emission of endogenous chromophores) and without photo-bleaching at biologically safe excitation/depletion power ranges in the NIR/visible spectral range. However, the gap between currently available super-resolution techniques and the requirements of life scientists is still large, and numerous aspects have to be addressed, such as deep-tissue penetration, pro-longed observation times, high frame rates, and bio-compatibility. Therefore, to decipher the mechanisms and kinetics of bio-related processes at the molecular level, widespread adoption of super-resolution and multiphoton microscopy requires more straightforward and inexpensive approaches to manipulating light below the diffraction limit.

2. Results and discussion

Here, we propose a simple method for sub-diffraction imaging based on the phenomenon known as photon avalanche.^[19,20] Unlike STED, this method uses a single excitation beam (obviating the need for a second depletion beam) and eliminates the aforementioned issues by

exploiting highly nonlinear optical nanomaterials that up-convert the frequency of light. Multi-photon imaging increases the resolution of light according to the equation:

$$\delta = \delta_0 / \sqrt{N} = \frac{\lambda}{2 \cdot NA \cdot \sqrt{N}} \quad \text{Equation 1}$$

where δ is the resolution, δ_0 is the single photon Abbe diffraction limited resolution, λ is the photoexcitation wavelength ($\lambda=1064$ nm is our case), NA is the numerical aperture of oil immersion microscope objective (typically $NA=1.4$), and N is the order of non-linearity, or the number of photons involved in the process. Sub-diffraction imaging is possible when $N \gg 1$ since intensity of multi-photon luminescence near the centre of the excitation beam spot will be enhanced relative to the intensity near its edges, due to the multiphoton luminescence intensity scaling as $I_{LUM} = P_{in}^N$, where P_{in} is the incident power density. While organic dyes and quantum dots exhibit reasonable multi-photon absorption cross sections suitable for e.g. 2-photon microscopy (Figure 1a), lanthanide-doped nanoparticles are even more attractive candidates for sub-diffraction microscopy since they can up-convert light with efficiencies over six orders of magnitude higher than multiphoton emitters (Figure 1b). This is because the up-conversion phenomenon in lanthanide doped nanoparticles exploits intermediate, metastable and real electronic levels to build the population of high energy states and generate high energy photons (Figure 1b, arrow 4) from multiple low energy NIR photons (Figure 1b, arrow 1). Demonstrating this non-linear concept with conventional up-converting lanthanide doped nanoparticles, Caillat et al. observed over 5-fold improvement in resolution during 4-photon upconversion imaging of single nanoparticles 20 nm to 50 nm in diameter.^[21] Further increases in resolution will be challenging, however, since 4-photon UC is rarely observed and higher-order UC will further decrease the efficiency while also producing UV light.

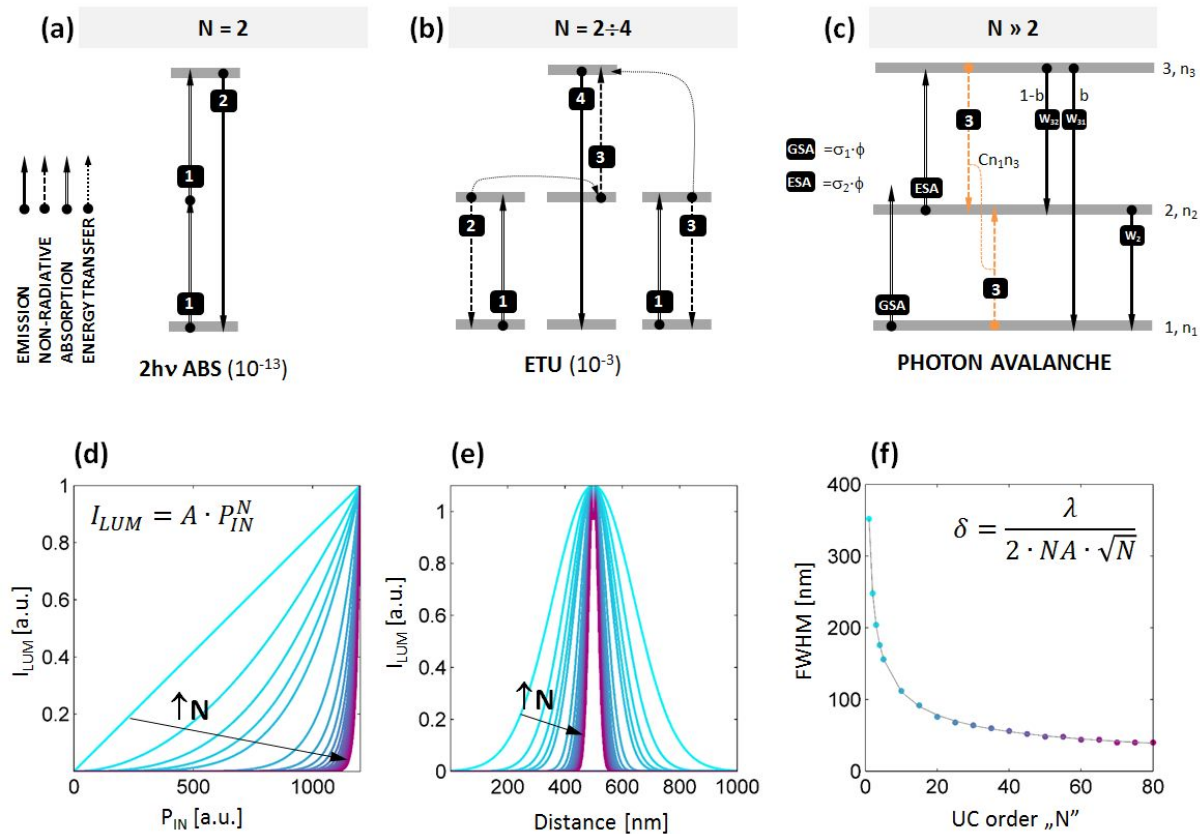


Figure 1. Introduction to photon avalanche emission and multi-photon super-resolution imaging. Schematic comparison of (a) two-photon absorption, (b) energy transfer upconversion (fr.Addition de Photons par Transferts d'Énergie, APTE) and (c) photon avalanche emission. The emission cross section for given transitions are shown in parentheses.^[22] Photon avalanche or looping requires negligible ground state absorption (GSA), significant excited state absorption (ESA), i.e. **ESA** \gg **GSA**, as well as efficient cross-relaxation (process 3) to promote ESA. (d-f) The impact of non-linearity of the luminescent label on the (d) photo-excitation power density dependence of emission, (e) the cross section of emission intensity $I_{LUM}(x)$ and (f) spatial resolution FWHM(N). The data were achieved by scanning a δ_0 wide diffraction-limited Gaussian beam (Equation 1, $\lambda=1064\text{nm}$, $NA=1.4$) across a single, non-linear, 10 nm diameter NPs, as a function of non-linearity strength (defined by N value) (colours on d-f are corresponding respectively).

To overcome the intrinsic limitations of multiphoton imaging with up-converting nanoparticles, we reasoned that an alternate up-conversion mechanism, photon avalanche (PA, schematically presented in Figure 1c), could be exploited to achieve higher nonlinearities than UCNPs exhibit and thus accomplish finer resolution. Photon avalanche is a highly nonlinear process with a very steep power dependence (e.g. $N=22$)^[23] that should shrink the Gaussian excitation spot profile of a laser scanning confocal microscope below the diffraction limit. PA process occurs in materials that have strong excited state absorption (ESA) but very weak ground state absorption (GSA). This combination is usually found when the excitation radiation is not resonant with the ground state transition but is resonant with ESA (see mechanism in Figure 1c). PA also requires electronic structure of the luminophore to facilitate “looping” of energy. This looping usually occurs through cross-relaxation (CR - process 3 in Figure 1c), in which a pair of single excited and single ground state ions produce two intermediately excited ions by donating part of the excited state energy to a ground state ion. If these intermediately excited ions can each absorb additional photons via ESA, the looping cycle can repeat, doubling the intermediate state population after every iteration of the loop. This produces a highly non-linear amplification of the light emitted by that state and other related states.

PA has been studied in Nd^{3+} ,^[23,24] Pr^{3+} ,^[25–27] Er^{3+} ,^[28] and Tm^{3+} ^{29–31} ions doped in bulk materials intended for solid-state lasers. The assignment of the PA mechanisms is typically supported by a characteristic “S”-shape emission intensity power dependence as well as the critical slowing down and power dependence of PA rise-times,^[32,33] exactly as has been numerically modelled in **Figure 2**. PA has mostly been observed at cryogenic temperatures, with only a few reports of PA at room temperature.^[19,32,33] There are even fewer studies of PA in nanoscale materials. In lanthanide-doped nanomaterials, looping and PA-like behaviour in Tm^{3+} doped materials have led to an expanded library of excitation wavelengths (e.g., 1064 nm, rather than the more typical ~800, 915 and 980 nm) that can be used for up-conversion

imaging, which have enabled super-resolution stimulated emission depletion based imaging^[16] and deep-tissue imaging.^[34] It is still debatable whether these “energy looping nanoparticles” exhibit PA since the strict definition of PA requires that $R = \sigma_{ESA}/\sigma_{GSA} < 10^{-4}$, where σ_{ESA} and σ_{GSA} are the absorption cross sections of ESA and GSA, respectively. Unfortunately, due to these strict requirements, complex electronic structure of lanthanide ions and large surface to volume ratio in nanomaterials, it is challenging to identify lanthanide dopant compositions that can host PA at biologically relevant temperatures.

We therefore used numerical solutions to coupled rate equations (Equation S1-S5, Supporting Information) to investigate whether Nd^{3+} -doped materials^[35-37] could be potentially used as PA sub-diffraction probes under physiologically relevant 1064 nm photoexcitation. The 1064 nm photons are, to a first approximation, not absorbed by Nd^{3+} ions from the ground $^4I_{9/2}$ state to the first metastable $^4F_{3/2}$ level due to significant $E(^4F_{3/2})-E(^4I_{9/2})-hc/\lambda \sim 2000 \text{ cm}^{-1}$ energy mismatch. Nevertheless, the 1064 nm photons match energy gap between the first excited state $^4I_{11/2}$ and the ground state $^4I_{9/2}$ manifolds. At increased temperatures, due to Boltzmann population, the $^4I_{11/2}$ level becomes occupied sufficiently to facilitate 1064 nm photoexcitation of $^4F_{3/2}$ level in Nd^{3+} ions, which has been shown to enable luminescent nanothermometry.^[38] There are few other reports of Nd^{3+} PA behaviour, e.g. lasing at 413 and 730 nm at temperatures $<40\text{K}$ under 603.6 nm in $LiYF_4$ single crystals.^[39] Nevertheless, the use of Nd^{3+} -doped nanomaterials as PA labels shall be considered as a representative case, with similar conclusions remaining valid for other dopant compositions that potentially host PA.

To understand the features and possible advantages of photon avalanche in Nd^{3+} , we studied the non-GSA-resonant excitation of Nd^{3+} ions, whose electronic structure is schematically presented in Figure 2a. Excitation at $\lambda_{exc}=1064 \text{ nm}$ is resonant with the ESA $^4I_{11/2} \rightarrow ^4F_{3/2}$ transition, while $\sigma_{GSA} \ll \sigma_{ESA}$ ($R=0.98 \cdot 10^{-4}$, see Supporting Information) at this wavelength for the $NaYF_4$ host. The $^4I_{11/2}$ level population can be achieved either by sideband

absorption or thermal population of this state. Upon rising excitation intensity, ESA may occur, and every absorbed photon can undergo either emission, non-radiative de-excitation or may transfer energy to other Nd^{3+} ions in the process of cross-relaxation. The emission follows the branching ratio characteristic (Figure S1, Supporting Information) for a given host; the 1064 nm and 880 nm emission lines correspond to ${}^4\text{F}_{3/2} \rightarrow {}^4\text{I}_{11/2}$ and ${}^4\text{F}_{3/2} \rightarrow {}^4\text{I}_{9/2}$, which populate the first excited state or the ground state, respectively. However, by increasing the number Nd^{3+} ions, faster cross-relaxation (W_{CR}) between the excited and ground states (${}^4\text{F}_{3/2}, {}^4\text{I}_{9/2} \rightarrow {}^4\text{I}_{15/2}, {}^4\text{I}_{15/2}$) of neighbor Nd^{3+} ions leads to doubling of the ${}^4\text{I}_{15/2}$ population. Aided by subsequent non-radiative processes (W_{NR}), the ${}^4\text{I}_{11/2}$ level population is doubled on every iteration of the loop. It is important to mention, some of these non-radiative processes (i.e. ${}^4\text{I}_{11/2} \rightarrow {}^4\text{I}_{9/2}$) may compete with the looping process, but this competition is already considered in the rate equation modelling by including non-radiative losses of ${}^4\text{I}_{11/2}$ population to the ground state. This sequence, in favourable host matrices (which define non-radiative rates) as well as dopant type and dopants concentration (which define looping strength), should in principle lead to a very steep relationship of emission intensity versus excitation intensity – i.e. high order nonlinearity, which is prerequisite for single excitation beam sub-diffraction imaging approach.

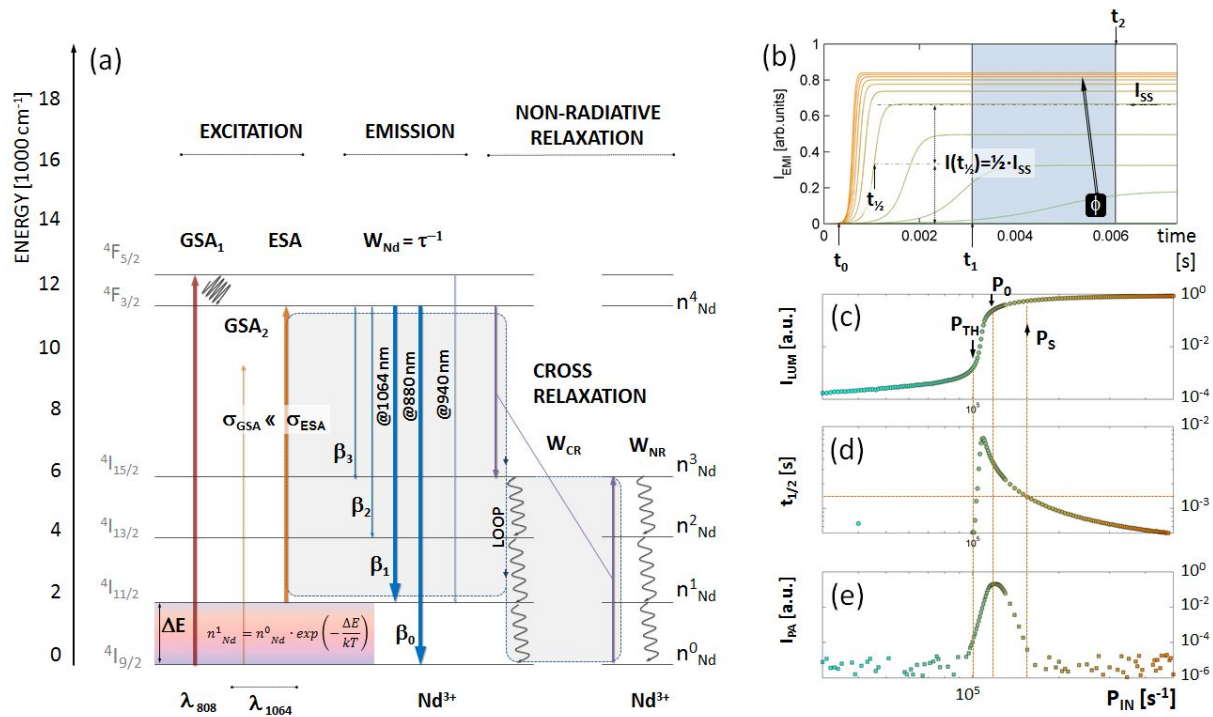


Figure 2. Explanation of fundamental features of photon avalanche based on energy diagram in Nd^{3+} ions doped nanomaterials under 1064 nm photo-excitation. (a) Energy diagram showing resonant (~ 800 nm) and non-GSA-resonant (~ 1064 nm) photoexcitation, radiative emission W_{Nd} from $4F_{3/2}$ level with its typical branching-ratios ($\beta_{0..3}$) and cross-relaxation (W_{CR}) that lead to recurrent populating the $4I_{11/2}$ level. Based on rate-equation numerical modeling, excitation intensity transients of $4F_{3/2}$ population rates ($I_{\text{EMI}} \cong n^4_{\text{Nd}}$) have been calculated; (b) power dependent (green to orange) temporal profiles of PA emission intensity achieved with the rate equation model in Nd^{3+} ions, together with graphically explained meaning of parameters ($I_{\text{SS}}, t_{1/2}, t_0, t_1, t_2$) used to further quantify the PA behavior; based on (b), either (c) steady-state photon avalanche (PA_S) population ($I_{\text{SS}} = I_{\text{LUM}}(t \rightarrow \infty)$), (d) half-rise time ($I_{\text{LUM}}(t_{1/2}) = 1/2 \cdot I_{\text{LUM}}(t \rightarrow \infty)$) and (e) the time gated photon avalanche (PA_G) photon counts ($I_{\text{PA}} = I_{\text{LUM}}(t_2) - I_{\text{LUM}}(t_1)$, where $t_0 < t_1 < t_2$ (blue area on (b)) are presented. The t_1 and t_2 were arbitrarily selected and such defined time “window” was kept fixed for all further simulations of rises-times and imaging.

Using the energy levels and possible transitions in Nd^{3+} activators shown in Figure 2a, we assembled a set of rate equations that describe the change in population for each of the energy levels in Nd^{3+} in time, after excitation pulse was applied at time t_0 . The rates of radiative and nonradiative transitions in Nd^{3+} (Equation 1-5, Supporting Information) are phenomenological factors (W_{NR} , W_{CR} , W_{Nd} , β explained above) included in the modeling as parameters. Next, these equations were numerically solved upon 1064 nm PA photoexcitation; kinetic profiles of the populations of the n^4_{Nd} level (Figure 2b) were calculated from solutions of calculations performed with different excitation intensities (i.e. $I_{\text{LUM}}(P_{\text{IN}}, t) = n^4_{\text{Nd}}$). Using *in silico* screening of these phenomenological parameters and excitation intensities, we identified conditions that are characteristic for photon-avalanche. The first characteristic feature is the “S”-shaped relationship between excitation (P_{IN}) and emission (I_{LUM}) intensity with a very steep photon avalanche region (Figure 2c) above PA threshold ($P_{\text{IN}} > P_{\text{TH}}$) and below saturation region ($P_{\text{IN}} < P_{\text{S}}$). The second feature is the slowing down of the rise-time ($t_{1/2}$) close to the PA threshold (Figure 2d). The time-dependent intensity profiles (Figure 2b) enabled us to determine steady-state up-conversion intensity (Figure 2b,c, $I_{\text{SS}} = I_{\text{LUM}}(P_{\text{IN}}, t \rightarrow \infty)$), half-rise time (Figure 2b,c, $t_{1/2} = t(I_{\text{LUM}}(P_{\text{IN}}, t) = 0.5 \cdot I_{\text{SS}})$) as well as the pure photon avalanche emission intensity (Figure 2d, $I_{\text{PA}} = I_{\text{LUM}}(P_{\text{IN}}, t_2) - I_{\text{LUM}}(P_{\text{IN}}, t_1)$, $t_2 > t_1$, where t_1 and t_2 are selected time points (explained below in more details), whose selection provides largest intensity contrast at the kinetic profile of PA emission (Figure 2b). The steady-state photon avalanche emission (PA_{S}) is achieved very slowly, because building a stable, steady-state population of emitting $^4\text{F}_{3/2}$ level (I_{SS}) requires tens of milliseconds when the excitation power is close to the PA photoexcitation intensity threshold (i.e. $P_{\text{TH}} < P_{\text{IN}} < P_{\text{S}}$). These values are over 10-fold longer than when excitation intensity (P_{IN}) is lower than the PA photo-excitation intensity threshold (linear or quadratic obsolete absorption) or higher than PA photo-excitation intensity saturation (efficient ESA). One may therefore find a time window (confined by t_1 and t_2 time points in Figure 2b), which discriminates PA photons

from conventional luminescence. The t_2 is the shortest time after switching on the PA threshold photoexcitation intensity ($P_{IN}=P_{TH}$) necessary to establish steady state emission, i.e. time t_2 at which $I_{LUM}(P_{TH}, t_2) = I_{LUM}(P_{TH}, t_2+\delta t)$ for $\delta t > 0$. The t_1 ($0 < t_1 < t_2$) is the time required to reach steady-state emission using excitation intensities close to saturation region, i.e. time t_1 at which $I_{LUM}(P_S, t_1) = I_{LUM}(P_S, t_1+\delta t)$ for $\delta t > 0$. In our simulations, both t_1 and t_2 were arbitrarily selected and kept fixed to 3 ms and 6 ms respectively for all data in all further experiments. Nevertheless t_1 and t_2 may be defined experimentally, by measuring half-rise-times (Figure 2d) to extract pure PA photons (Figure 2e). Once selected for given PA-NPs, t_1 and t_2 may be used for all further experiments. The difference between time-gated photon avalanche intensity (PA_G) counts at t_1 and t_2 quantifies the number of photons occurring exclusively due to the photon avalanche phenomenon. This metric enables us to determine the origin of emitted photons and assign them as originating from either PA or ESA phenomenon. Consequently, not only the I_{PA} (Figure 2e) can be used to get rid of sample autofluorescence, but most of all enables to determine optimal P_0 to avoid saturation and is of pivotal importance for extreme non-linearities and thus for single beam super-resolution imaging.

We next sought to determine whether Nd^{3+} could exhibit PA with sufficient non-linearity to increase imaging resolution. A steep power dependence in principle should shrink the width of the diffraction limited Gaussian excitation spot down to tens of nanometers if the critical excitation intensity P_0 (Figure 1d-f) is fixed properly below the saturation region ($P_0 < P_S$). To test the resolution of a PA-enabled scanning microscope, we calculated spatially resolved intensity profiles of a single 10 nm diameter NP (**Figure 3a**, dark grey) scanned with a diffraction limited Gaussian beam, which based on Equation 1 has a full width at half maximum equal to $FWHM = \lambda/2 \cdot NA = 1064 \text{ nm}/2 \cdot 1.45 = 367 \text{ nm}$. At excitation intensities under which the optical response of the NP is linear (i.e. $I_{LUM} \sim P_{IN}$), the emission intensity profile retains the Gaussian shape of the excitation spot (Figure 3a, red). When the response is

quadratic, as in up-conversion or 2-photon absorption (i.e. $I_{LUM} \sim P_{IN}^N$, $N=2$), the intensity profile narrows by $N^{0.5}$, or by ca. 1.4-fold (Figure 3a, orange). If one further increases the power factor N , as is the case with e.g. 3rd or 4th order of Tm^{3+} blue or violet up-conversion, respectively³¹, the resulting intensity profile further narrows down to a ~ 1.7 and 2-fold reduced sub-diffraction spot. Up to $N=4$, photon up-conversion can be relatively efficiently generated in known UC materials, but higher orders are beyond reach of typical UCNPs phenomenon. Interestingly, we proposed and demonstrated *in silico* that N can be further increased without going to UV spectral range, using photon avalanche (Figure S3d,f, Supporting Information) to further narrow the emission spot cross-section size (Figure 1 d-f). Based on Equation 1 (with $\lambda=1064$ and $NA=1.4$), a high non-linearity of $N = 10$ improves the optical resolution by over 3 times down to ~ 116 nm and $N = 80$ results in enhancements as large as 9-fold to reach ~ 41 nm optical resolution (Figure 1f, Figure S2, Supporting Information).

Notably, we found that to achieve such improvement in resolution, one must carefully select the excitation beam intensity. Because the S-shaped photon avalanche power dependence (Figure 2c) contains a steep, power-dependent region between P_{TH} and P_S ($P_{TH} < P_{IN} < P_S$) ‘surrounded’ by a relatively flat ($N < 3$) in-out dependence, the ultimate spatial resolution will depend on selection of P_0 (Figure 2c, Figure 3a (blue lines)) as well as the composition and type of the host material (Figure 3b-f). Selecting an excitation intensity outside these optimal P_0 value results in the 10 nm NPs being imaged as a much larger object (Figure 3a, medium and thick navy blue curve). However, as discussed below in greater detail, the optimal P_0 narrows the cross-section profile far below diffraction limit (Figure 3a, thin line). Such Photon Avalanche Single beam Super-resolution Imaging (PASSI) therefore has the potential to realize single-excitation-beam, sub-diffraction limited imaging. This in turn should significantly simplify the apparatus for super-resolution imaging by eliminating the need to

spatially align the beams and the need to synchronize the excitation or depletion pulses (in non-CW mode).

The performance of PA nanomaterials depends on a few phenomenological parameters defined in the model. For example the cross-relaxation rate (W_{CR}) depends on distance between doping ions and thus should depend on dopants concentration as well as host type (Figure 3c-d). The non-radiative de-excitation rate (W_{NR}) is a host-dependent factor, which should be lower in e.g. fluorides than in oxides, and also depends on the energy gap ΔE between respective levels (Figure 3e-f). The variability of the looping strength (W_{CR} , green to blue on Figure 3c-d) and excitation intensity impacts not only the emission intensity but also affects the full width half maximum (FWHM) of the cross section of the emission profile from single 10 nm nanoparticle. Raising the dopant concentration (increasing W_{CR}) flattens the power dependence of the S-shaped curve (Figure 3c), which degrades the spatial resolution (enlarges the FWHM, Figure 3b), but also widens the acceptable range of I_0 required for sub-diffraction limited imaging. The radiative rate ($W_{Nd} = 1/\tau_R$) can be easily determined by experimental measurement (at low temperature and low dopants concentration) of luminescence decay. W_{Nd} , as well as the branching ratio ($\beta_{0..3}$) from the $^4F_{3/2}$ level are a host dependent parameters (see Figure S1, Supporting Information). For example, the $\beta_{0..3}$ parameter defines the statistical distribution of emitted photons between $^4F_{3/2} \rightarrow ^4I_J$ ($J=9/2, 11/2, 13/2, 15/2$, correspondingly) multiplets and may be estimated based on Judd-Ofelt theory for a given host matrix.^[40,41] Therefore, we hypothesize that selecting proper host material, dopants and dopant concentration will enable the optimization of lanthanide doped nanoparticles aiming to achieve photon avalanche in nanomaterials. Due to numerous differences in the optical properties of nanoparticles relative to bulk crystals, this may be a challenging task. However, as soon as PA phenomenon is demonstrated in nanomaterials, sub-diffraction imaging can potentially be demonstrated in a simple and affordable way.

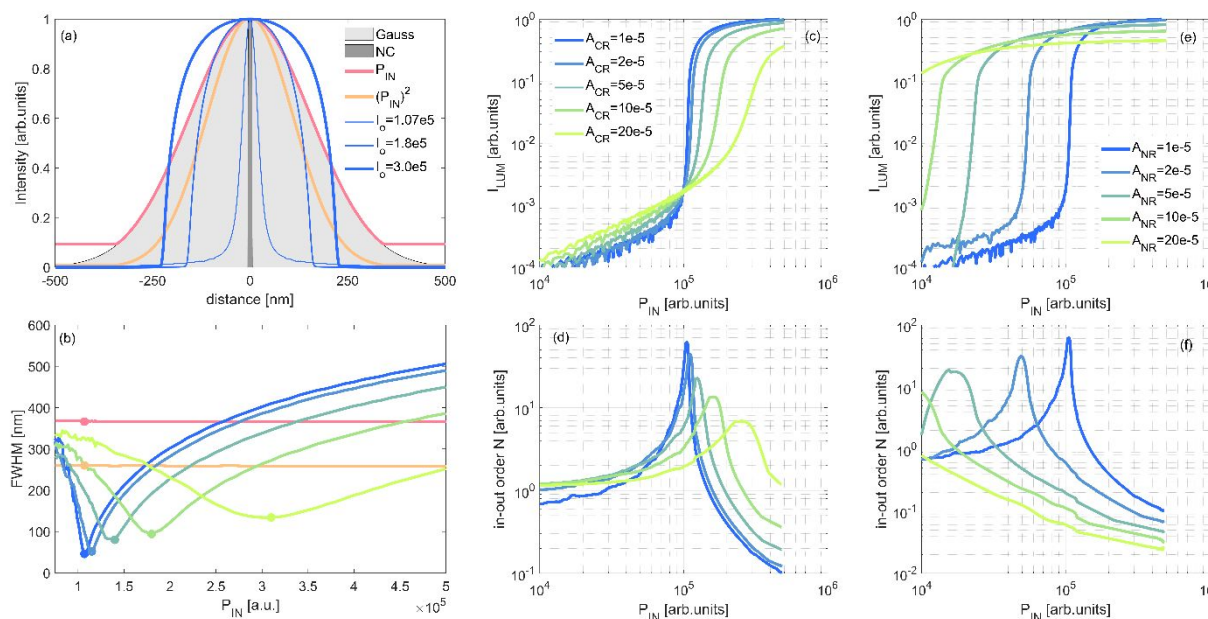


Figure 3. The impact of PA parameters on spatial resolution enhancement. (a) Comparison of cross section of a single $\phi = 10$ nm PA NP (dark grey) measured with a diffraction limited Gauss spot (light grey Gauss profile FWHM ~ 330 nm and under different conditions of power dependent relationship (Linear $I_{LUM} \sim P_{IN}$ - red, quadratic $I_{LUM} \sim (P_{IN})^2$ - orange, and photon avalanche S-shaped in-out relationships ($A_{CR} = 1 \cdot 10^{-5}$; $I_0 = 1.07 \cdot 10^5$, $1.8 \cdot 10^5$, $3 \cdot 10^5$ – thin, medium and thick blue curves respectively). (b) Comparison of the full width half maximum (FWHM) of the intensity profiles of 10 nm PA NPs for linear (red) and quadratic (orange) in-out emission-excitation dependence (Equation 1) and at different PA excitation intensity and CR rate, using different S-shaped in-out curves obtained at (c) different concentration of Nd^{3+} dopants A_{CR} ($A_{CR} = 1, 2, 5, 10$ and $20 \cdot 10^{-5} s^{-1}$) and (e) for different non-radiative rate. Panels (d) and (f) present non-linear factors N for data presented on panel (c) and (e) as calculated based on algorithm available in Supporting Information.

To determine the optical resolution of the proposed system, we used our model to simulate the imaging of a phantom composed of three PA NPs of 10 nm diameter with variable distance between them (**Figure 4a**, cross sections at fixed distances – **Figure 4b**). The three NPs are

indistinguishable when separated by less than 30 nm, but for distances larger than 40 nm (Figure 4b) the NPs become easily resolvable. These results depend on the host materials parameters (Figure S3, Supporting Information) and excitation intensity (Figure S3, Figure S4, Supporting Information). Next, we employed a Gaussian excitation beam to image a 2D phantom *in silico* (Figure 4c), simulating images produced by conventional linear confocal microscopy (Figure 4d) as well as images produced by the steady state (Figure 4e) and time gated photon avalanche (Figure 4f) imaging of 10-nm Nd³⁺-doped nanoparticles. Optimal parameters of excitation beam and NPs composition were taken from above described *in silico* studies (i.e. intensity $P_0=1.075 \cdot 10^5$; $W_{CR}=1 \cdot 10^5$) and from the time gated data ($t_1=3\text{ms}$, $t_2=6\text{ms}$) defined in Figure 1b.

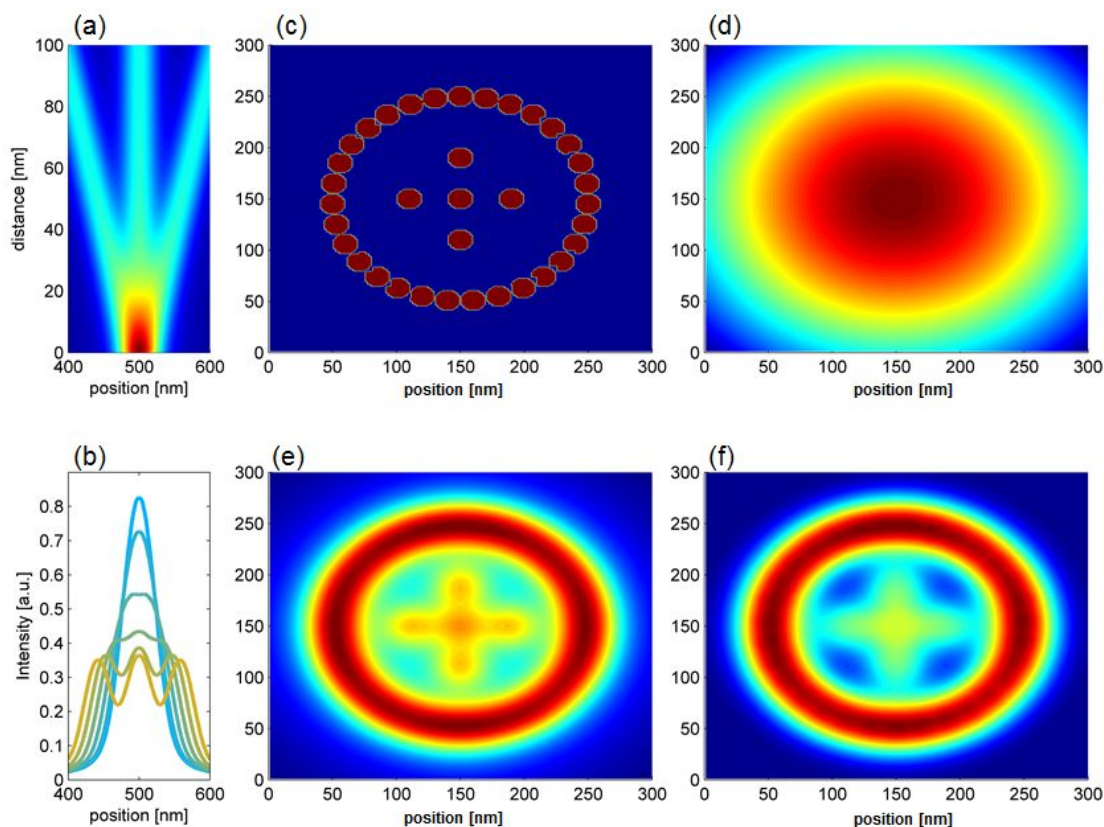


Figure 4. Spatial resolution enhancement using photon avalanche labels. (a) Phantoms composed of 3 NPs ($\phi=10$ nm PA NPs) placed at different distances (y axis) are reconstructed using optimal conditions ($A_{CR}=1 \cdot 10^{-5}$, $I_0=1.07 \cdot 10^5$), and (b) respective cross sections of graph (b) for distances of 5, 10, 20, 30, 40 and 50 nm between the Nd³⁺-doped NPs. (c) Phantom

composed of 10 nm PA NPs reconstructed with (d) linear, (e) steady state avalanche and (f) time-gated avalanche models (graphs d,e,f are normalized to their local maxima, cross section across e and f are presented in Figure S4, Supporting Information).

Based on the qualitative information from Figure 4 and more detailed analysis of cross sections along the centre of the simulated images (Figure S5, Figure S6, Supporting Information) one may conclude that the steady state photon avalanche imaging is better suited to distinguish the closely spaced NPs (Figure S5, Figure S6- top, Supporting Information), while the pure photon avalanche time gated photons (PA_G) are providing lower background signal, but also lower contrast of closely spaced NPs (Figure S5, Figure S6- bottom, Supporting Information). The obvious drawback of the postulated PA in super-resolution applications comes from the absolute intensity, which is at least an order of magnitude weaker than the up-conversion itself, but the simulations clearly demonstrated that linear “confocal-like” imaging (Figure 4d) cannot distinguish individual NPs on the same phantom. Therefore, although weaker, the signal to background of PA imaging should be beneficial in terms of its spatial resolving power and imaging contrast. Another great advantage of PASSI imaging is the fact no pinhole is required. This is because PA emission occurs only at the exact center of the focal volume, which makes the out-of-focus background signal to be very low and thus not detectable, either in X-Y as well in axial Z plane (Figure S7, Supporting Information). For this reason, the optical system does not require complex nor costly solutions, neither in excitation nor detection path, and eventually conventional confocal laser scanning microscopes (LSM) shall prove to be effective systems easily adoptable to PASSI imaging mode.

The advantage of PASSI is that it is a simple solution to technical challenges that currently limit the wide adoption of existing super-resolution methods. First, it enables operation with only one photoexcitation beam, enabling parallel excitation over multiple spots

or the simultaneous detection of multiple colors. The long rise-times of intensities in PA process will enable, through time gated detection, elimination of the background and sample autofluorescence signals. All these features will enable radical improvements in the signal to noise ratio while also increasing penetration depth into scattering or heterogeneous media, which are important for ultrasensitive detection in complex biological samples. Although PA in nanomaterials has been rarely reported, lanthanide doped nanoparticles have been extensively studied for over a decade, and their synthesis, characterization and on-demand design are reproducible and relatively well understood. The major advantages of PA labels with respect to biological applications stem from fundamental properties of lanthanide ions, which include extreme photo-stability, narrowband and multiple absorption/emission as well as large Stokes shift, efficient anti-Stokes emission and ultimately photoexcitation at a single line from robust and affordable laser diodes. Moreover, long wavelength photoexcitation (e.g. 1064 nm for Nd, Tm etc.) where organic molecules do not absorb nor emit photons provides low background auto fluorescence signal and low scattering of exciting photons. This feature is extremely important for the safety of imaging for biological samples – i.e. no excessive exposure of living sample occurs to photon flux, thus no thermal or photobleaching side effect are expected. The discussed PA model revealed that finding the most appropriate excitation intensity to enhance the sub-diffraction resolution can be done experimentally, because the PA threshold correlates well with longest PA rise-time. Importantly, PA based super-resolution imaging is compatible with existing and widely available fluorescent microscopy techniques - in particular, any laser scanning confocal microscope (LSCM) can easily perform PASSI by employing PA nanoparticles and adopting precise control over excitation intensity.

Conclusion

The *in silico* modeling of the photon avalanche phenomenon in Nd³⁺-doped dielectric NPs demonstrates that their steep power dependence and slow rise-times, which are characteristic for PA emission, may become key enabling elements of a simple and affordable method for photon-avalanche assisted single beam super-resolution imaging (PASSI). The critical parameter to make the proposed system useful is the knowledge of excitation intensity at which saturation begins (Figure 2c, P_0), which can be easily derived experimentally due to the exceptional slowdown of the rise time in the PA regime (Figure 2). It is important to note that the P_0 will be lower than typically used in other lanthanide-doped NPs, which is advantageous in light of the laser safety exposure thresholds for living cells. These features make PA interesting not only in terms of their fundamental physics, but also because of its technical simplicity and ability to parallelize the actions by multi-spot sub-diffraction imaging (e.g. as known from Nipkov confocal discs).

According to our modeling, PASSI confines the emission point spread function (PSF) to 3-8 times lower volume than conventional confocal PSF without using a depleting beam, without complicated beam overlap adjustments, and without temporal synchronization of the pump and depletion beams. Sub-diffraction limited imaging is an obvious application for this technology and any confocal microscope with appropriate excitation wavelength and spectral filters can perform super-resolution imaging with PASSI without extensive modification. The use of 1064 nm photoexcitation has been shown to be advantageous for biomedical applications due to reduced scattering and autofluorescence under such excitation. Increased observation depths, prolonged observation times, and multi-colour labels under single excitation are also possible with lanthanide-doped nanomaterials.

Future effort is needed to synthesize optimized nanoparticles and provide experimental evidence for the validity of our predictions as well as to evaluate the sensitivity and master the

working conditions for the proposed phenomena to occur. Typically, UCNPs are synthesized with diameters around $\sim 25\text{nm}$, but relatively brighter sub 10-nm Ln^{3+} highly doped UCNPs have been already demonstrated⁴². Despite intense research, the surface bio-functionalization of UCNPs still requires reliable protocols to make the UCNPs suitable for bio-specific labeling. The overall size of such constructs should be therefore similar to conventional fluorescently labeled antibodies. The PA phenomenon in nanomaterials may be difficult to observe due to large surface quenching (to be potentially diminished by NP surface passivation) and the requirement for room temperature operation. But little effort has been exerted so far to optimize the Ln^{3+} nanomaterials for room-temperature PA operation. Fortunately, the physical model relates the *in silico* variables to the phenomenological parameters, such as radiative and non-radiative rates of cross-relaxation and emission. These suggested parameters should guide experimental explorations into the most appropriate host matrix, dopants and concentrations. As soon as photon avalanche is achieved in nanomaterials, their unique photo-physics will lead to an extraordinary array of applications – including sub-diffraction imaging, sensing, multi-functional labeling and theranostics for biomedical applications, as well as photonic applications such as optical computing, optical switching, data storage – all of which will benefit from such high optical nonlinearities.

Supporting Information

Supporting Information is available from the Royal Society of Chemistry or from the author.

Acknowledgments.

Work at the Molecular Foundry was supported by the Office of Science, Office of Basic Energy Sciences, of the U.S. Department of Energy under Contract No. DE-AC02-05CH11231. KP acknowledges the support from Foundation for Polish Science (FNP) under START programme. L.M. acknowledges the support from NCN OPUS 14 under grant UMO-2017/27/B/ST5/02557.

Received: ((will be filled in by the editorial staff))

Revised: ((will be filled in by the editorial staff))

Published online: ((will be filled in by the editorial staff))

References

- [1] G. Vicidomini, P. Bianchini, A. Diaspro, *Nat. Methods*. **2018**, *15*, 173.
- [2] C. Wu, T. Schneider, M. Zeigler, J. Yu, P. G. Schiro, D. R. Burnham, J. D. McNeill, D. T. Chiu, *J. Am. Chem. Soc.* **2010**, *132*, 15410.
- [3] E. D'Este, D. Kamin, F. Göttfert, A. El-Hady, S. W. Hell, *Cell Rep.*, **2015**, *10*, 1246.
- [4] F. Helmchen, W. Denk, *Nat. Methods*, **2005**, *2*, 932.
- [5] N.G. Horton, K. Wang, D. Kobat, C.G. Clark, F.W. Wise, C.B. Schaffer, C. Xu, *Nat. Photonics*, **2013**, *7*, 205.
- [6] L. Schermelleh, R. Heintzmann, H. Leonhardt, *J. Cell Biol.*, **2010**, *190*, 165.
- [7] B. Huang, H. Babcock, X. Zhuang, *Cell*, **2010**, *143*, 1047.
- [8] K. I. Willig, B. Harke, R. Medda, S.W. Hell, *Nat. Methods*, **2007**, *4*, 915.
- [9] G. Vicidomini, G. Moneron, K.Y Han, V. Westphal, H. Ta, M. Reuss, J. Engelhardt, C. Eggeling, S. W. Hell, *Nat. Methods*, **2011**, *8*, 571.
- [10] A. Schönle, S.W. Hell, *Nat. Biotech.*, **2007**, *25*, 1234.
- [11] H. Bock, C. Geisler, C.A. Wurm, C. von Middendorff, S. Jakobs, A. Schönle, A. Egner, S.W. Hell, C. Eggeling, *Appl. Phys. B Lasers Opt.* **2007**, *88*, 161.
- [12] D. Jin, P. Xi, B. Wang, L. Zhang, J. Enderlein, A. M. van Oijen, *Nat. Methods*, **2018**, *15*, 1.
- [13] T. Ha, P. Tinnefeld, *Annu. Rev. Phys. Chem.*, **2012**, *63*, 595.
- [14] R. Kolesov, R. Reuter, K. Xia, R. Stöhr, A. Zappe, J. Wrachtrup, *Phys. Rev. B*, **2011**, *84*, 1.
- [15] Q. Zhan, H. Liu, B. Wang, Q. Wu, R. Pu, C. Zhou, B. Huang, X. Peng, H. Ågren, S. He, *Nat. Commun.* **2017**, *8*, 1058.
- [16] Y. Liu, Y. Lu, X. Yang, X. Zheng, S. Wen, F. Wang, X. Vidal, J. Zhao, D. Liu, Z. Zhou, C. Ma, J. Zhou, J. A. Piper, P. Xi, D. Jin, *Nature*, **2017**, *543*, 229.
- [17] C. Chen, F. Wang, S. Wen, Q. P. Su, M. C. L. Wu, Y. Liu, B. Wang, D. Li, X. Shan, M. Kianinia, I. Aharonovich, M. Toth, S. P. Jackson, P. Xi, D. Jin, *Nat. Commun.* **2018**, *9*, 4.
- [18] Q. Wu, B. Huang, X. Peng, S. He, Q. Zhan, *Opt. Express*, **2017**, *25*, 30885.
- [19] M. F. Joubert, S. Guy, B. Jacquier, *Phys. Rev. B*, **1993**, *48*, 10031.
- [20] R. Scheps, *Prog. Quantum Electron.*, **1996**, *20*, 271.
- [21] L. Caillat, F. Pellé, B. Hajj, V. Shynkar, D. Chauvat, J. Zyss, *Conference on Lasers and Electro-Optics Europe and International Quantum Electronics Conference*,

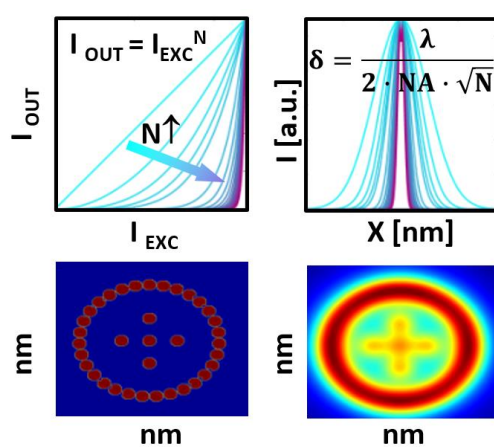
CLEO/Europe-IQEC, 2013

- [22] F. Auzel, *Chem. Rev.*, **2004**, *104*, 139.
- [23] H. Deng, S. Yang, S. Xiao, H. M. Gong, Q. Q. Wang, *J. Am. Chem. Soc.*, **2008**, *130*, 2032.
- [24] M. F. Joubert, S. Guy, B. Jacquier, *Phys. Rev. B*, **1993**, *48*, 10031.
- [25] S.Kück, A.Diening, E.Heumann, E.Mix, T.Sandrock, K.Se bald, G.Huber, *J. Alloys Compd.* **2000**, *300*, 65.
- [26] M. E. Koch, A. W. Kueny, W. E. Case, *Appl. Phys. Lett.*, **1990**, *56*, 1083.
- [27] J. S. Chivian, W. E. Case, D. D. Eden, *Appl. Phys. Lett.* **1979**, *35*, 124.
- [28] A. Brenier, A. M. Jurdyc, *J.Lumin.* **1996**, *69*, 131.
- [29] R.M. Macfarlane, R. Wannemacher, T. Hebert, W. Lenth, Upconversion laser action at 450.2 and 483.0 nm in Tm:YLiF₄, Optical Society of America, Baltimore, Maryland United States, 1990.
- [30] V. François, F. Pellé, P. Goldner, D. Simkin, *J. Lumin.*, **1995**, *65*, 57.
- [31] T. Hebert, R. Wannemacher, R. M. MacFarlane, W. Lenth, *Appl. Phys. Lett.*, 1992, *60*, 2592.
- [32] M. F. Joubert, *Opt. Mater.*, **1999**, *11*, 181.
- [33] M. F. Joubert, S. Guy, S. Cuerq, P. A. Tanner, *J.Lumin.*, **1997**, *75*, 287.
- [34] E. S. Levy, C. A. Tajon, T. S. Bischof, J. Iafrati, A. Fernandez-Bravo, D. J. Garfield, M. Chamanzar, M. M. Maharbiz, V.S. Sohal, P. J. Schuck, B.E. Cohen, E. M. Chan, *ACS Nano*, **2016**, *10*, 8423.
- [35] A. Bednarkiewicz, D. Wawrzynczyk, M. Nyk, W. Strek, *Opt. Mater.* **2011**, *33*, 1481.
- [36] D. Wawrzynczyk, A. Bednarkiewicz, M. Nyk, W. Strek, M. Samoc, *Nanoscale* , **2012**, *4*, 6959.
- [37] A. Bednarkiewicz, D. Wawrzynczyk, M. Nyk, W. Strek, *Appl. Phys. B Lasers Opt.* **2011**, *103*, 847.
- [38] L. Marciniak, A. Bednarkiewicz, K. Elzbieciak, *J. Mater. Chem. C*, **2018**, *6*, 7568.
- [39] W. Lenth, R. M. M. Macfarlane, *J. Lumin.* **1990**, *45*, 346.
- [40] G. S. Ofelt, *J. Chem. Phys.* **1962**, *37*, 511.
- [41] B. R. Judd, *Phys. Rev.* **1962**, *127*, 750.
- [42] D. J. Gargas, E. M. Chan, A. D. Ostrowski, S. Aloni, M. Virginia, P. Altoe, E. S. Barnard, B. Sani, J. J. Urban, D. J. Milliron, B. E. Cohen, P. J. Schuck, *Nat. Nanotechnol.* **2014**, *9*, 300.

TOC Entry

Photon avalanche in lanthanide doped nanoparticles for biomedical applications: super-resolution imaging

Artur Bednarkiewicz, Emory Chan, Agata Kotulska,
Lukasz Marciniak, Katarzyna Prorok



Photon avalanche in lanthanide doped nanoparticles show exceptional properties, potentially suitable for single photoexcitation beam sub-diffraction imaging.